Journal of Molecular Liquids 313 (2020) 113401

Contents lists available at ScienceDirect

Journal of Molecular Liquids

journal homepage: www.elsevier.com/locate/molliq

Rheological and flow birefringence studies of rod-shaped pigment nanoparticle dispersions

Péter Salamon [a,*], Yong Geng [b], Alexey Eremin [c], Ralf Stannarius [c], Susanne Klein [d], Tamás Börzsönyi [a]

[a] Institute for Solid State Physics and Optics, Wigner Research Centre for Physics, P.O. Box 49, H-1525 Budapest, Hungary
[b] School of Polymer Science and Engineering, Qingdao University of Science and Technology, Qingdao 266042, China
[c] Otto-von-Guericke Universität Magdeburg, Institute of Physics, D-39016 Magdeburg, Germany
[d] Centre for Fine Print Research, University of the West of England, Bower Ashton Studios, Kennel Lodge Road, Bristol BS3 2JT, United Kingdom of Great Britain and Northern Ireland

ARTICLE INFO

Article history:
Received 16 April 2020
Received in revised form 15 May 2020
Accepted 19 May 2020
Available online 01 June 2020

Keywords:
Rheology
Viscoelasticity
Flow-induced birefringence
Nanoparticle suspensions
Colloids
Liquid crystals

ABSTRACT

We study rheological and rheo-optical properties of suspensions of anisometric pigment particles in a non-polar fluid. Different rheological regimes from the dilute regime to an orientationally arrested gel state were characterized and compared with existing theoretical models. We demonstrate the intricate flow behaviour in a wide range of volume fractions. A unique combination of the optical properties of the particles results in a giant rheo-optical effect: an unprecedentedly large shear stress-induced birefringence was found in the isotropic range, exhibiting a sharp pre-transitional behaviour.

1. Introduction

Colloidal suspensions, i.e. dispersions of solid particles in liquids, are important in many fields of our life including biology, pharmaceutics, food, cosmetic and paint industries. They often show complex non-Newtonian behaviour, and the rheology of such systems has been of interest for a long time [1]. There is a vast variety of suspensions and their properties strongly depend on the dispersion medium and the type of the suspended particles [2,3]. Besides the viscosity of the solvent, the concentration, size, and shape of the particles and the interactions between them are the most important parameters determining their rheological behaviour [4]. The coupling between the optical properties of a fluid and the flow is particularly interesting. Especially in case of complex fluids, such as colloidal suspensions formed by anisometric particles, flow-induced birefringence indicates interactions leading to the alignment of particles in the flow.

Shearing isotropic soft materials can lead to the emergence of optical anisotropy [5–10]. It is observed as birefringence and dichroism describing retardation and attenuation of the transmitted light, respectively. Flow-induced birefringence, the so-called Maxwell effect, was observed in many types of isotropic materials including suspensions of rod-like particles [11–13], polymer melts [5] and solutions [14–16], emulsions [17,18], and small molecular [19], and polymeric liquid crystalline materials [20,21].

In this work, we present the rheological and rheo-optical properties of suspensions of anisometric dichroic pigment nanoparticles Pigment Red 176 (PR176) in the nonpolar solvent n-dodecane. These suspensions have been shown to exhibit several remarkable features [22–27] such as (i) formation of an orientationally ordered nematic-like phase at a volume fraction (of the particles) as low as 0.17 (for photos of textures see Refs. [23, 24, 27]), (ii) strong electro-optical response in the isotropic state, (iii) electric field-induced reversible phase separation [25], and (iv) electric field and light-induced pattern formation [26] with a variety of morphologies. The patterns were found to exhibit complex relaxation dynamics related to material flow. These features have to be attributed primarily to the pronounced prolate shape of the suspended crystallites. We address here the flow behaviour and rheology of this system, in relation to the ordering of the anisometric particles.

The colloidal suspensions studied here contain particles with a moderate aspect ratio (around 10). Such materials are represented in the literature less frequently than more slender types like nanotubes, rod-like polymers or viruses. We compare the rheological and visco-elastic properties of the suspensions under study with theoretical models. We quantify the shear-induced birefringence, and find an unusually large effective stress-optical coefficient.

* Corresponding author.
E-mail address: salamon.peter@wigner.hu (P. Salamon).

https://doi.org/10.1016/j.molliq.2020.113401

2. Flow-induced birefringence

In order to mathematically describe flow-induced birefringence, let us consider the usual notation [7], where direction 1 is along the flow, direction 2 is parallel to the gradient, and direction 3 is the neutral one perpendicular to 1 and 2 in the laboratory coordinate system. The principal axes of the stress tensor are denoted by I, II, and III, respectively. Considering an assumption that the principal axes of the stress tensor coincide with those of the refractive index ellipsoid, one can arrive to a stress-optical rule formulated as

$$\Delta n = (n_I - n_{II}) = C(\sigma_I - \sigma_{II}) = C\Delta\sigma, \quad (1)$$

where Δn, C, and $\Delta\sigma$ are the birefringence, the stress-optical coefficient, and the tensile stress, respectively. In experiments, one may observe a deviation of the optical extinction direction from the flow direction, expressed by the extinction angle χ. Flow alignment often occurs in sheared nematics [28,29] or in granular materials consisting of elongated particles [30].

It can be shown that

$$2\sigma_{12} = \Delta\sigma \sin 2\chi, \quad (2)$$

where $\sigma_{12} = \sigma$ is the shear stress and χ is the extinction (or alignment) angle. In order to determine C, one has to know the shear stress σ, birefringence Δn and χ.

Strictly, the validity of the stress-optical rule is not expected in suspensions of elongated particles, because the total stress is the sum of three different terms, even in a simplified picture considering spheroids dilutely suspended in a Newtonian fluid. Following the description in Ref. [1](p.282), the total stress is the sum of the elastic contribution from Brownian motion, the viscous stress from the drag of the solvent on the ellipsoids (derived by Hinch and Leal [31]), and the stress form the Newtonian fluid.

Moreover, it is important to note that for suspensions of rod-like (and also disk-like) particles, the emergence of the nematic phase can be expected above a critical volume fraction as shown by Onsager [32] and later by others using more sophisticated models [33,34]. First, usually, the higher order liquid crystalline phase is in thermodynamic equilibrium with the isotropic phase forming a biphasic system [35–48]. Increasing the volume fraction, the ratio of the liquid crystal phase increases until it is the only phase present. For thermotropic mesogens, it was shown that the nematic phase can be induced by shearing the isotropic phase [49–51].

3. Experimental

The suspensions under study were prepared using a blue shade benzimidazolone pigment (Pigment Red 176 - PR176). The chemical structure of PR176 is shown in Fig. 1a. The preparation method of the suspensions was similar to the one employed in previous studies [23,25]. A commercially available form of PR176, namely Novoperm Carmine HF3C (Clariant, Frankfurt am Main, Germany), was used, in which the primary particles were prolate [24] with characteristic dimensions for their length, width and thickness of 322±160 nm, 63± 21 nm and 17.3±11 nm, respectively (see Fig. 1b). The aspect ratio p_a=9.8 is given by dividing the length by the geometric mean of the smaller dimensions. The particles of PR176 were suspended in the non-polar solvent dodecane with a commercially available polymeric dispersant Solsperse 11200 (Lubrizol, Brussels, Belgium, used as received). We note that Solsperse 11200 contains 50 wt% solvent (de-aromatized white spirit) and 50 wt% polymeric dispersant. This polymer adsorbs at the surface of the particles leading to a steric repulsive interaction between them. First, suspensions with pigment concentrations of c_w=20 wt% (and above) were prepared by milling. An amount of 70 wt% of dispersant of PR176 was added to the solvent. Then, after the addition of the pigment, the mixture was milled in a planetary mill (Fritsch Pulverisette 7 premium line), using 0.3 mm yttria-stabilized zirconia beads in zirconia-lined pots for 60 min at 500 rpm. The temperature inside the pots was always kept below 60 °C, using appropriate cooling cycles. Concentrations below 20 wt% were prepared by the dilution of the initial high concentration suspensions. The stability of the suspensions was tested by centrifugation at 10000 rpm for 60 min. Furthermore, the samples with various concentrations did not show any phase separation or aggregation even after 12 months.

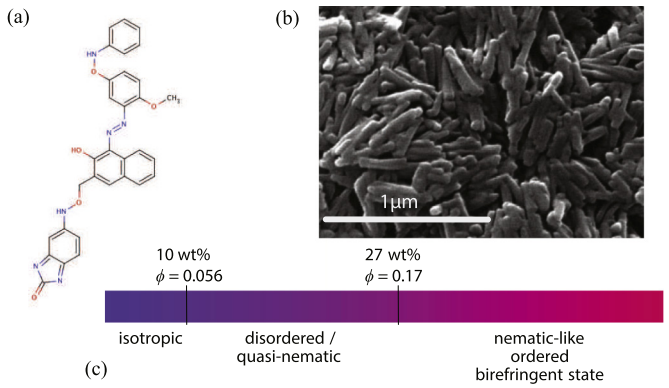

Fig. 1. (a) The molecular structure of Pigment Red 176; (b) The scanning electron microscope (SEM) image of the pigment particles; (c) Phase diagram of Pigment Red 176 dispersion in dodecane [23].

The volume fraction ϕ of particles in the suspensions was calculated from the weight concentrations using the densities ρ_c = 1402 kg/m^3, ρ_d = 840 kg/m^3, and ρ_s = 746 kg/m^3 of the pigment particles, the dispersant, and the solvent, respectively. In our experiments, suspensions with 1, 5, 10, 15, 20, 25, 30, 35 and 40 wt% of the pigment particles were used, which correspond to the volume fractions ϕ = 0.005, 0.027, 0.056, 0.087, 0.119, 0.154, 0.191, 0.23, and 0.272, respectively. We note that the ϕ values above correspond to the volume fractions of the particles without the polymeric layers of the dispersant. Using the same materials, it was shown by small angle neutron scattering (SANS) experiments [52] that the effective volume fraction increment of the pigment particles due to the presence of the dispersant is negligible. The thickness of untreated Novoperm Carmine was found to be 21.4 ± 0.2 nm with a polydispersity of 64%. With this value, the surface area of the particles was calculated and then 6.5 mg/m^2 of dispersant were added. About 3.69 ± 0.07 mg/m^2 were adsorbed and the SANS measurements showed that the thickness of the particles stayed roughly the same: 20.3 ± 1.9 nm, but the variation on the polydispersity had increased. In case of a slightly different pigment, neutron reflection measurements were performed showing that the thickness of the adsorbed polymer is about 3 nm. The measurements also showed that there is a dynamic equilibrium between adsorption and desorption. Based on these findings, we conclude that the volume fraction of the particle with adsorbed dispersant can be approximated by the volume fraction of the untreated particle, especially since the surface is not covered densely.

The phase diagram is shown in Fig. 1c, where the isotropic phase lies in the range of few weight percent of the particles, the optically responsive disordered phase occurs at intermediate concentrations, and the orientationally aligned nematic-like state emerges at high particle content. This phase is globally isotropic without long-range orientational order, but has short-range orientational correlations fluctuating in time in the form of clusters of submicron size [23].

The rheological investigations were carried out using an Anton Paar MCR 502, equipped with a Peltier-based temperature regulator plate and a hood. All measurements were done at T=30°C, with a temperature accuracy better than 0.1 K. The basic rheological characterization of the pigment suspensions with different concentrations was done in

rotational and oscillatory modes. In the rotational mode, the viscosity was measured as a function of shear rate by a cone-plate measuring system of 60 mm diameter with the cone angle 0.5° (CP60), and additionally by using a parallel-plate measuring system of 43 mm diameter (PP43) with transparent upper and lower glass plates. The existence and the range of linear viscoelasticity was first determined in oscillatory mode by measuring the dynamic elastic moduli G', G'' as a function of the oscillation amplitude at a fixed angular frequency using PP43. Then at a sufficiently low amplitude in the linear regime, G' and G'' were measured as functions of the angular frequency. To avoid transient effects, a dwell period of at least 30 min between the filling the sample and the measurement was chosen.

Influences of ageing, thixotropy, and other time dependent phenomena were examined, and could be ruled out. Successive shear rate sweeps (without dwell) yield the same results. The birefringence of the samples was measured as a function of the shear rate concurrently with the viscosity measurement (using PP43). The sketch of the optical setup is presented in Fig. 2a. The beam of a diode laser with the wavelength λ=657.3 nm was first polarized at an angle of −45° with respect to the x-axis, defined by the velocity of the rotating (upper) plate at the place of incidence. Then, the beam entered the hood, propagated through the sheared sample, and was modulated with a Hinds Instruments photoelastic modulator (PEM) with the modulation axis set parallel to the x-axis. The modulation frequency was 42 kHz. The light path continued through the second polarizer (analyzer) adjusted to +45° to the x-axis. Finally, a signal from a photomultiplier (PM) proportional to the transmitted laser intensity was measured by a Tiepie HS3 oscilloscope. The oscilloscope was triggered by the 1st harmonic reference output of the PEM. The apparent optical retardation was determined by a well-established method using:

$$\tilde{\Gamma} = \arctan\left(\frac{I_{1f}J_2(\Gamma_0)}{I_{2f}J_1(\Gamma_0)}\right), \tag{3}$$

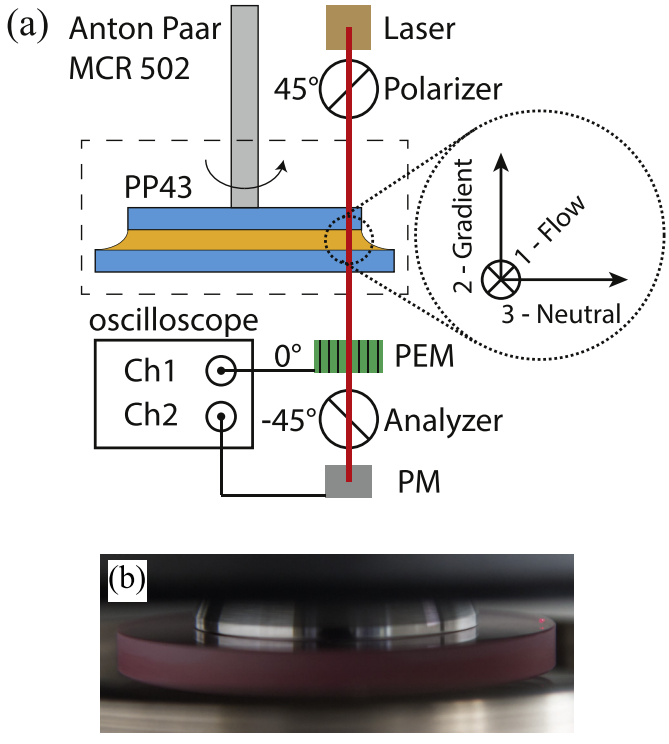

Fig. 2. (a) The schematic figure of the optical setup to determine the effective birefringence as a function of shear rate. (b) The parallel plate measuring system (PP43) illuminated through by the laser beam.

where I_{1f}, I_{2f} are the amplitudes of the 1st and 2nd harmonics of the intensity signal, $J_{1,2}$ are Bessel functions of the first kind, and Γ_0=2.407 is the retardation modulation amplitude of the PEM. I_{1f} and I_{2f} were determined from the oscilloscope data numerically in Labview using the lock-in principle. $\tilde{\Gamma}$ is related to the actual optical retardation Γ by $\Gamma = \tilde{\Gamma} + m\pi$, where m is an integer to be determined from the experiment (see below). The effective birefringence in the 1–3 plane was calculated by:

$$\Delta n_{13} = \frac{\Gamma\lambda}{2\pi d}, \tag{4}$$

where d is the local gap of the rheometer cell. We note that the dichroism of the measured sample influences only the dc level of the transmitted intensity, the first and second harmonics are left unaffected. Consequently, the effective birefringence values, determined with the present method, are not influenced by the dichroism of the system.

4. Results and discussion

The relative viscosity η_r (i.e. the viscosity of the suspension normalized by the viscosity of the solvent) is presented as a function of the shear rate $\dot{\gamma}$ for pigment suspensions with lower (a) and higher (b) volume concentrations in Fig. 3. The suspensions show an increasing shear thinning character [1,2,53–58] with increasing concentration. Up to ϕ=0.119 and below the shear rate of 10 s^{-1}, the change in η is rather small, thus the dispersions appear to have Newtonian plateaus in the low Péclet number ($Pe = \dot{\gamma}/D_r$) limit [59,60]. Here D_r is the rotational diffusion constant. At higher shear rates, shear thinning becomes more pronounced, i.e. the slope of the viscosity curves decreases stronger with increasing $\dot{\gamma}$. In the measured shear rate range, the pigment suspensions did not exhibit a Newtonian plateau at high Pe.

At ϕ=0.154 and above, the behaviour is different: the decrease of viscosity as a function of $\dot{\gamma}$ grows even at very low shear rates, clearly showing the lack of a low Pe Newtonian plateau. Especially in the cases of the three largest volume fractions, the $\dot{\gamma}$ dependence of the viscosity appears to obey a power law. This type of behaviour was observed in other concentrated systems such as rod-like polymer solutions [61–64], and suspensions of rod-like cellulose micro/nanocrystals [65–68] and was attributed to the elasticity of a polydomain nematic defect structure.

We note that Fig. 3b includes two datasets for ϕ=0.191, resulting from the measurements using the parallel-plate and the cone-plate measuring systems. The advantage of the cone-plate system is the uniform shear rate in the cell. However, this geometry suffers from occasional jamming of the suspensions near the contact region that affect the measurements, therefore the parallel-plate geometry is simpler from a practical point of view. For parallel-plates, $\dot{\gamma}$ is defined as the average shear rate, which is two-thirds of the shear rate at the circumference of the plate [69]. We note that there is another correction method for the inhomogeneous shear rate, described in Ref. [57](Eq. (5.5.10)), which results in approximately the same. It can be clearly seen that the two systems gave similar results, therefore for higher volume fractions, we used only the parallel plate for easier sample filling. It is notable that at high concentration the viscosity strongly increases with concentration, e.g. increasing the volume fraction by about 0.04 results in an order of magnitude higher viscosity.

In order to investigate the effect of the polymeric dispersant, we measured the flow curve of the mixture of 28 wt% Solsperse in dodecane (with no particles). In this concentration, the amount of dispersant corresponds to the highest concentration nanoparticle dispersion (40 wt%, ϕ=0.272). The above mixture was found to exhibit Newtonian rheology with about 10 mPas viscosity as seen in Fig. 3b denoted as “Solsperse”. This finding means that the dispersant itself does not affect much the viscosity even at relatively high concentration.

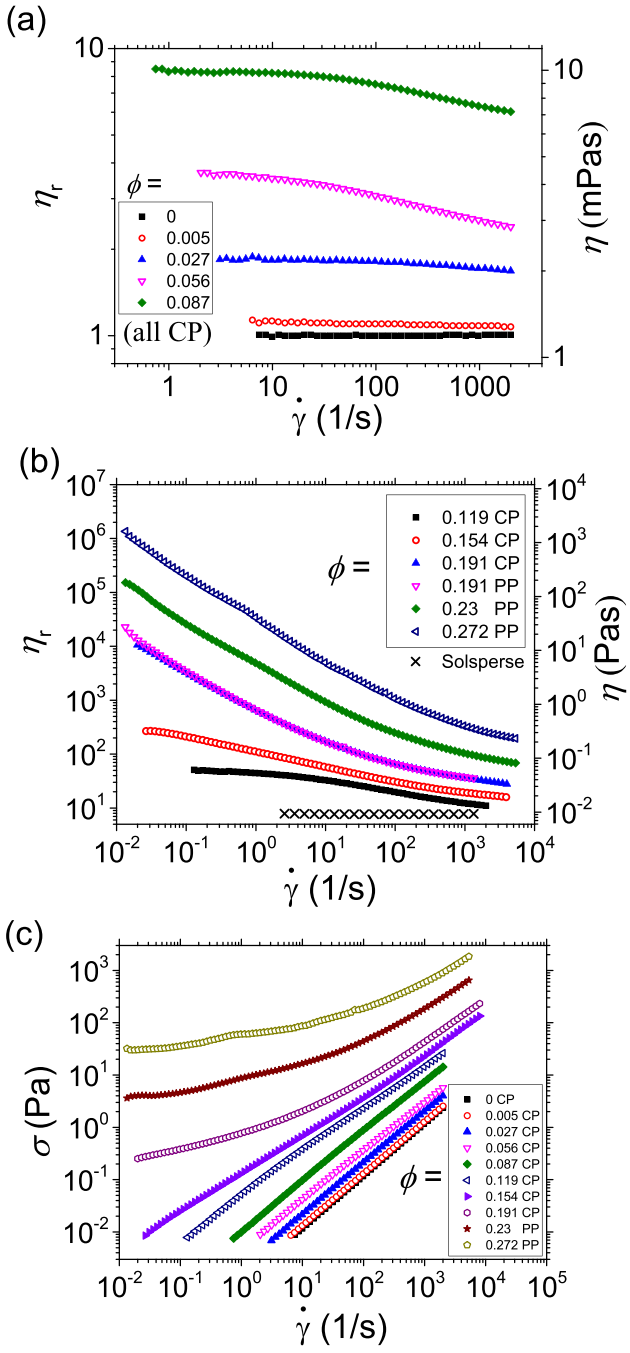

Fig. 3. The viscosity as a function of shear rate in suspensions of (a) lower, and (b) higher volume concentrations of elongated pigment nanoparticles; data for 28 wt% mixture of Solsperse dispersant in dodecane. (c) The shear stress as a function of shear rate. Measurements done with a cone-plate (CP) and a parallel-plate (PP) system in the volume fraction ranges $\phi \le 0.191$ and $\phi \ge 0.191$, respectively.

In Fig. 3c, the shear stress σ is shown as a function of the shear rate. Seemingly, in the concentrated suspensions (ϕ>0.16), a residual stress remains even at very low values of $\dot{\gamma}$, which manifests a yielding behaviour.

The viscosity as a function of the volume fraction is presented in Fig. 4. Data are shown for the low shear rate limit, i.e. for each concentration, the lowest point in Fig. 3 was used (solid black squares), and for high shear rates, i.e. 2000 s^{-1} (open red circles), corresponding to low and high *Pe*, respectively. In the low Pe branch, from ϕ=0 to 0.272, η_r increases by about 6 orders of magnitude, while for high Pe, the viscosity change is less than three orders of magnitude.

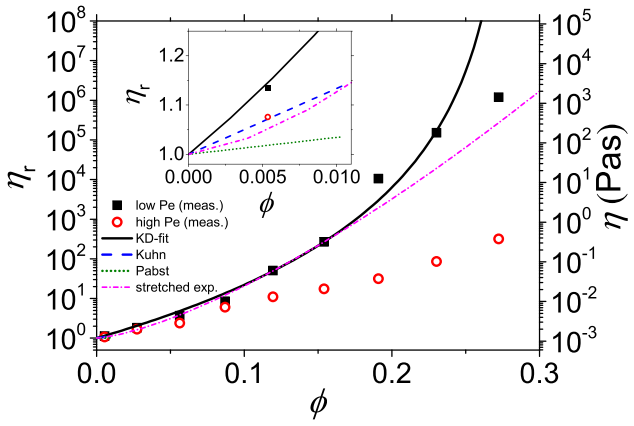

Fig. 4. The viscosity of suspensions as a function of the volume fraction ϕ of the elongated pigment nanoparticles. The data shown were measured at the lowest possible shear rate (solid black squares - low *Pe*) and at a high shear rate of 2000 s^{-1} (open red circles - high *Pe*). Theoretical predictions for suspensions of ellipsoids with the aspect ratio of 9.8 for the low and high *Pe* limits are included for comparison (blue dashed line - Kuhn, and green dotted line - Pabst, respectively.) Fits of the Krieger-Dougherty-equation, and a stretched exponential are also given (black solid line and magenta dash-dotted line, respectively). The inset shows the same data focusing on the low concentration range.

Generally, the concentration dependence of the viscosity can be described by various models. The Krieger-Dougherty [70] equation is the most widely used empirical formula, which is to fit in the low *Pe* range:

$$\eta_r = \left(1-\frac{\phi}{\phi_m}\right)^{-[\eta]\phi_m}, \tag{5}$$

where $[\eta] = \lim_{\phi\to 0}(\eta_r-1)/\phi$, and ϕ_m is a fit parameter often called the maximum volume fraction of the particles. Furthermore, $[\eta]$ denotes the intrinsic viscosity, a measure of the particles contribution to the viscosity in the zero concentration limit. Another approach is to use a stretched exponential [71,72]:

$$\eta_r = e^{a\phi^{\nu}}, \tag{6}$$

where a and ν are fit parameters.

As it is seen, our low Pe data can be fitted well by both the Krieger-Dougherty equation and a stretched exponential in the low-concentration range. The fits resulted in the following parameters: ϕ_m=0.28(± 0.06) and $[\eta]$=25(± 12) for Eq. (5), a=79(± 15) and ν=1.4(± 0.1) for Eq. (6). Though the fit values we found are unusual, yet such are not unprecedented. For wollastonite microparticles, the maximum packing fraction and the intrinsic viscosity was found to be 0.13 and 10.2, respectively [73]. For hematite rods (aspect ratio: 8.4), maximum packing fraction was found to be as low as 0.12, while the Krieger-Dougherty fit resulted in 23 for the intrinsic viscosity [74]. The high fitted value of intrinsic viscosity indicates that the interactions between particles are additional to hydrodynamic forces.

For elongated particles, an analytic expression was derived by W. and H. Kuhn [75] for the zero-shear viscosity of suspensions of relatively low aspect ratio $1<p_a<15$ rigid Brownian ellipsoids:

$$\eta_r = 1+\phi\left(2.5+0.4075(p_a-1)^{1.508}\right). \tag{7}$$

More recently, using the results of Brenner [76], Hinch and Leal [31], and Scheraga [77], Pabst et al. [73] calculated the intrinsic viscosity in the $Pe \to \infty$ limit, for suspensions of prolate spheroids in the regime $1<p_a<50$ that resulted in:

$$\eta_r = 1+\phi\left(2.5+0.123(p_a-1)^{0.925}\right). \tag{8}$$

The fitted intrinsic viscosity is found to be considerably larger compared to suspensions of isometric particles ($[\eta] \sim 2.5 - 3.5$) [78,79], as

expected. However, both analytic formulas for anisometric particles give smaller viscosities than the viscosity of our pigment suspension, as it is seen in Fig. 4. The deviation may be attributed to the relatively large polydispersity of the particles and, as a result, the uncertainty in the aspect ratio and the calculated volume fraction. Moreover, the applied models consider hard spheroids, which describes our system only approximately, because of the grafting polymer layers on the surfaces of the particles and the triaxial ellipsoid shape of the latter.

Qualitatively similar stationary rheological behaviour was presented earlier in various types of other elongated particle suspensions. Aqueous suspensions of cellulose nanoparticles were investigated by several groups. Araki et al. [4,80] investigated dilute particle dispersions with high aspect ratio (~50), and the measured intrinsic viscosity of non-aggregated systems was consistent with the analytical formula of Simha [81,82]. Similar systems [83–85] but with longer particles (larger p_a) were studied even in the region of high volume fractions. In that work, the transition from the isotropic to the nematic phase was observable as a slight decrease in the viscosity, followed by a steep increase up to the largest concentrations, where a power law dependence of η_r vs. $\dot{\gamma}$ was found, similarly to our system. Also, in aqueous dispersions of colloidal hematite rods (p_a=8.4 [74]), qualitatively similar rheology was shown. However, the parameter ($[\eta] \times \phi_m$) in the Krieger-Dougherty fit was found to be lower: ~3 compared to ~7, the value in the case of pigment suspensions. This difference may arise from the different level of electrostatic interactions between particles. We assume that the ionic strength in the aqueous dispersions was much higher compared to our system that uses a nonpolar solvent.

In order to characterize the viscoelastic properties of the suspensions, we performed oscillatory shear measurements in the parallel plate geometry. The resulting storage and loss moduli (G' and G'', respectively) were determined at a constant angular frequency ω=10 rad/s, as a function of the shear strain γ. At lower concentrations (ϕ<0.119), the suspensions were found to be liquid-like with no measurable elasticity. At ϕ=0.119 (see Fig. 5a), a nonzero storage modulus was measured; both moduli showed only a slight dependence on strain. Thus the suspension exhibits a linear viscoelasticity in the measured range up to γ=100%. At a higher concentration of ϕ=0.154 (see Fig. 5b), G' and G'' become larger, but their relative difference is getting

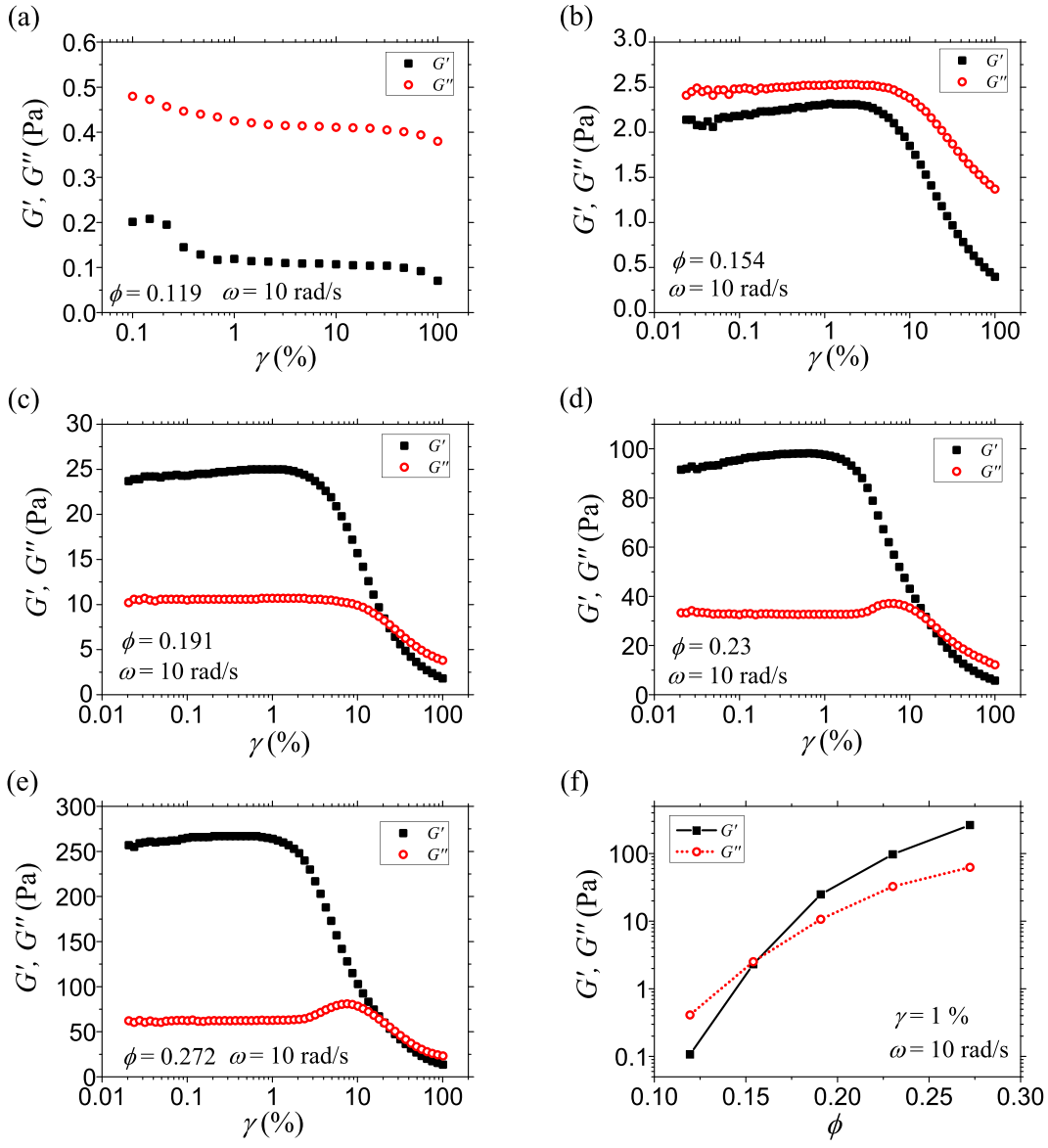

Fig. 5. (a–e) The storage (G') and loss (G'') moduli as a function of shear strain γ, in the volume fraction range ϕ = 0.119–0.272 of the elongated pigment nanoparticles in dodecane. (f) The ϕ dependence of the viscoelastic moduli measured at γ=1%. The oscillatory measurements were done at constant angular frequency ω=10 rad/s.

smaller, indicating a more pronounced gel-like behaviour. The linear viscoelastic range breaks down at around γ=2%, where both moduli start to decrease. As seen in Fig. 5c, increasing the concentration up to ϕ=0.191 results in a more gel-like system with a strongly increasing G' in the linear viscoelastic regime. At the highest concentrations (for ϕ=0.23, and ϕ=0.272, see Fig. 5d and e, respectively), the increasing trend of the moduli continues, and after the breakdown of the linear viscoelastic regime, a peak in $G''(\gamma)$ becomes observable, showing that our highly concentrated suspensions clearly exhibit a soft glassy response [86]. The concentration-dependent change in the viscoelasticity of suspensions can be followed in Fig. 5f, where G' and G'' are plotted versus ϕ measured at ω=10 rad/s and γ=1% in the linear viscoelastic regime. The transition from viscoelastic liquid-like to gel-like behaviour occurs at a critical volume fraction at around ϕ=0.16.

The storage and loss moduli measured in the linear viscoelastic regime as a function of the angular frequency ω are shown for three selected volume fractions in Fig. 6. For ϕ=0.119 the two curves describing the frequency dependence of G' and G'' run almost parallel in the entire range, showing fluid-like behaviour. Earlier calculations and measurements showed that the viscoelasticity of dilute rod-like suspensions can be described by a modified Maxwell-model with a crossover frequency at several kHz. Interestingly, at ϕ=0.154, the values of G' and G'' are almost equal for the whole ω-range. Above ϕ=0.154, the suspensions turn to be gel-like i.e. the storage modulus becomes higher than the loss modulus, in accordance with results presented in Fig. 5. As an example, the case ϕ=0.272 is shown in Fig. 6, where seemingly the difference between G' and G'' is also independent on ω. In the present range of measurements, the data can be approximated by a power law, where the exponent is smaller at lower volume fractions. This power-law-like behaviour seems to prevent a plausible comparison with classical descriptions such as the Mountain-Zwanzig equation [1,87] that relates the storage modulus in the high frequency limit to the inter-particle interactions, because of the lack of frequency independent high frequency limit of G'.

The apparent optical phase difference $\tilde{\Gamma}$ as a function of local shear rate was determined using Eq. (3). The measurements were done in the parallel plate geometry, where the actual shear rate depends linearly on the radius from the rotation axis. In order to compare the measured optical properties to the shear stress, the local shear rate has to be used, which is denoted by $\dot{\gamma}_L$ (determined from the location of the laser spot with respect to the rotation axis). The measured value of $\tilde{\Gamma}$ as a function of $\dot{\gamma}_L$ is shown in Fig. 7 for two volume fractions. Fig. 7a shows the data for ϕ=0.119, the tendency of the curve is typical for low volume fractions. $\tilde{\Gamma}$ is restricted to the range of $-\pi/2$ to $+\pi/2$, because it is obtained from the inverse tangent in Eq. (3). The actual phase shifts outside of this interval can be determined if the following assumptions hold: 1) Γ changes smoothly (as a function of $\dot{\gamma}_L$), 2) there is one reference point, where the absolute value of Γ is known. In the regime $\phi \le 0.119$, at the lowest shear rates, Γ is zero, therefore, we assume that the measured $\tilde{\Gamma}$ is equal to Γ (0th order), until it reaches $+\pi/2$ and continues from $-\pi/2$ in the 1st order.

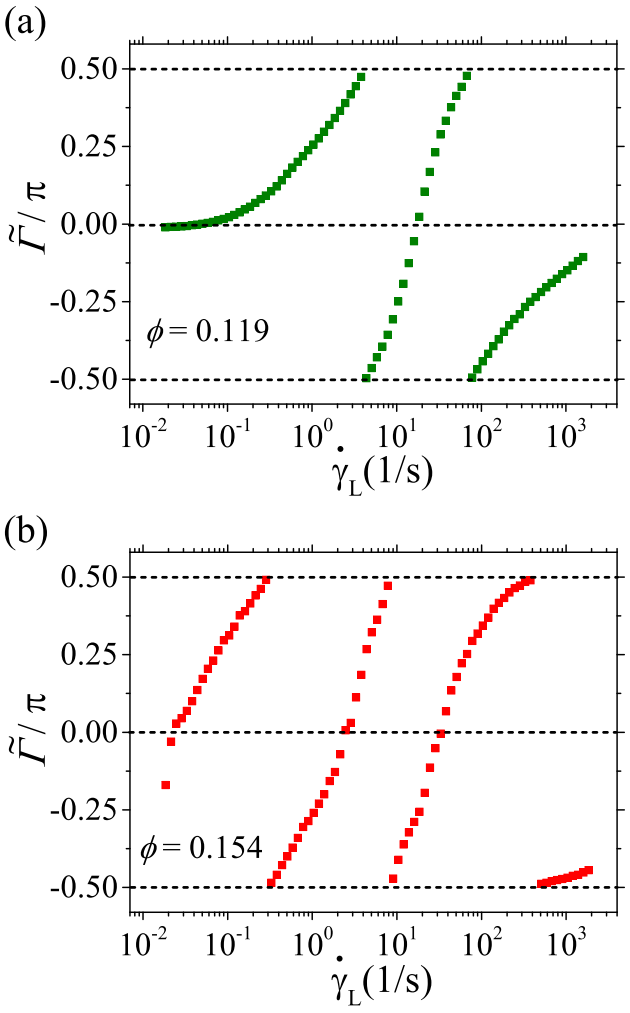

Fig. 7. The measured apparent phase difference between the ordinary and extraordinary light rays as a function of shear rate at the light path () in the case of different volume fractions ϕ of the elongated pigment nanoparticles dispersed in dodecane: (a) ϕ=0.119, (b) ϕ=0.154.

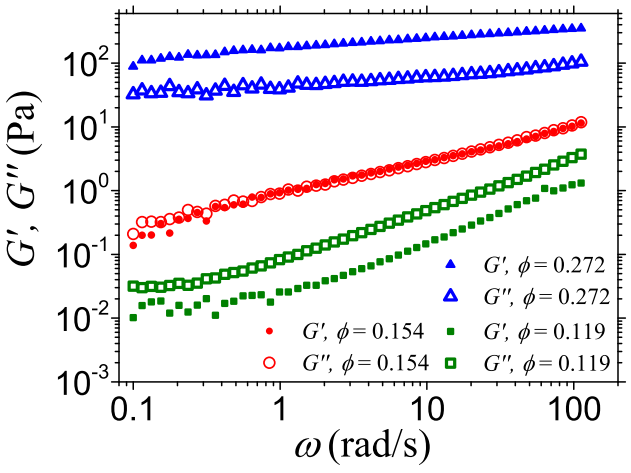

Fig. 6. The storage (G') and loss (G'') moduli as a function of angular frequency ω, for three suspensions of the elongated pigment nanoparticles in dodecane with the volume fractions ϕ = 0.119, 0.154, and 0.272. The viscoelastic moduli were measured in the linear viscoelastic regime.

In Fig. 7b, one can see that at the lowest $\dot{\gamma}_L$, Γ is not exactly zero, and the increase with $\dot{\gamma}_L$ is much sharper compared to the lower concentration cases. This is in accordance with the rheological results, where both the gelation and the occurrence of the nematic-like phase were found to emerge at around $\phi \approx 0.16$. At higher concentration, there is considerable birefringence present already in absence of shear, owing to the residual birefringence of the dispersion and the presence of randomly oriented birefringent domains in the laser spot. Therefore no reference point can be identified, and the absolute level of Γ cannot be determined.

In the following, we aim to give a phenomenological description of our results that may be useful to make comparison with systems described by a stress-optical coefficient. We are aware of that a stress-

optical rule may not strictly be applicable in our system, nevertheless we derive an effective stress-optical coefficient denoted by C^*. We follow the notations introduced in Section 2. Since our probe light beam propagates in direction 2, only an effective birefringence could be measured in the 1–3 plane: Δn_{13}. This is related, however, to the refractive indices and to the extinction angle assuming uniaxial symmetry by

$$\Delta n_{13} = \frac{n_I}{\sqrt{1 + \left(\frac{n_I^2 - n_{II}^2}{n_{II}^2}\right) \sin^2 \chi}} - n_{II}, \tag{9}$$

where n_I and n_{II} are the principal refractive indices. Using $\Delta n = (n_I - n_{II})$ and assuming that Δn is very small, in first order one obtains:

$$\Delta n_{13} \approx \cos^2 \chi \, \Delta n. \tag{10}$$

Combining Eqs. (1), (2), and (10) leads to:

$$\Delta n_{13} \approx C^* 2\sigma \frac{\cos^2 \chi}{\sin 2\chi} = \cot \chi C^* \sigma, \tag{11}$$

which can be reduced to the simple form:

$$\Delta n_{13}|_{\sigma \to 0} \approx C^* \sigma \tag{12}$$

if one assumes $\chi = \pi/4$, which is a good approximation in the limit $\sigma \to 0$ [7]. Consequently, using Eq. (12), we can determine the effective stress-optical coefficient by taking the slope of the $\sigma(\Delta n_{13})$ curve in the origin. Using the shear stress - shear rate data from the measurements by the cone-and-plate system (see Fig. 3c) and Eq. (4), the sigma dependence of Δn_{13} is plotted in Fig. 8a for various volume concentrations.

It can be seen that a linear stress-birefringence relation can only be found at the onset of the curves at relatively low values of σ, which is not surprising, since the assumption above of $\chi = \pi/4$ stands only in the zero-shear limit. Even in the case of the lowest concentration suspension ($\phi = 0.005$), there is measurable shear-induced birefringence. After the sharp initial increase in Δn_{13}, the birefringence tends to saturate. The nonlinear character of Δn_{13} with increasing shear stress is a consequence of the stress dependence of χ and Δn (see Eq. (10)).

In order to investigate the effect of the polymeric dispersant, we measured the birefringence as a function of shear stress in the mixture of 28 wt% Solsperse in dodecane (with no particles). As seen in Fig. 8 (denoted as "Solsperse"), no detectable level of flow-induced birefringence was found in spite of that in this concentration, the amount of dispersant corresponds to the highest concentration nanoparticle dispersion (40 wt%, ϕ=0.272). This finding refers to that the dispersant itself has negligible contribution in the large flow-induced birefringence found in the nanoparticle dispersions.

In Fig. 8b, we plotted Δn_{13} divided by ϕ as a function of σ to check whether the curves of the effective birefringence versus stress collapse or not. Seemingly, the curves collapse to some extent, however the overlap between them is not perfect, meaning that this simple rescaling does not completely explain the ϕ dependence of the rheo-optical data. Nevertheless, one may notice on Fig. 8b that the extrapolation of the curves to the high stress side may give a birefringence value corresponding to ϕ=1 (the solid crystal material of nanoparticles) with assuming perfect alignment of the particles to the flow, being roughly 0.055, which value may not be unrealistic.

In order to demonstrate the effect of concentration on the shear-induced birefringence close to saturation, we plotted Δn_{13} taken at $\dot{\gamma}_L = 1000\ s^{-1}$, as a function of ϕ in Fig. 9. A monotonic, almost linear increase was found. Since the birefringence of a particulate suspension in an isotropic fluid depends linearly on both the orientational order parameter and the concentration of the particles, the value of Δn_{13} at a constant shear rate ($1000\ s^{-1}$) is expected to linearly increase with the particle concentration. A similar situation occurs in binary suspensions of

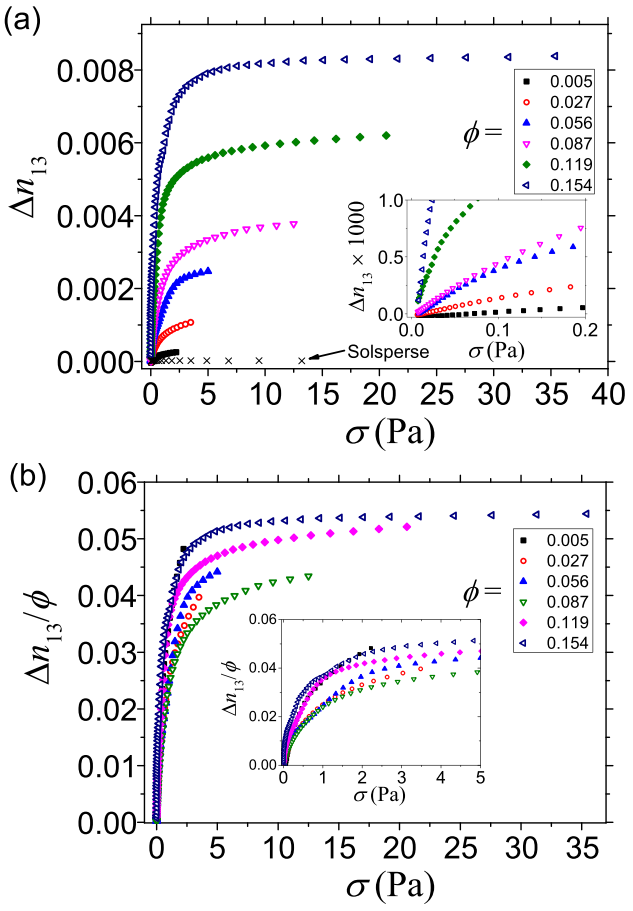

Fig. 8. (a) The measured effective optical anisotropy Δn_{13} as a function of shear stress σ in the case of pigment nanoparticle suspensions in dodecane with different ϕ volume fractions; data for 28 wt% mixture of Solsperse dispersant in dodecane. The linear part of Δn_{13} versus σ at the origin was used to determine the effective (zero-shear) stress-optical coefficient C^* (inset). (b) The measured effective optical anisotropy Δn_{13} per volume fraction as a function of shear stress.

pigment and magnetic nanoparticles, where an external magnetic field induces chain formation of magnetic particles leading to an alignment of nonmagnetic pigment rods [27]. The saturating value of the birefringence appears to scale linearly with concentration.

The effective stress-optical coefficients determined by Eq. (12) are presented in Fig. 9 as a function of the volume fraction. In the

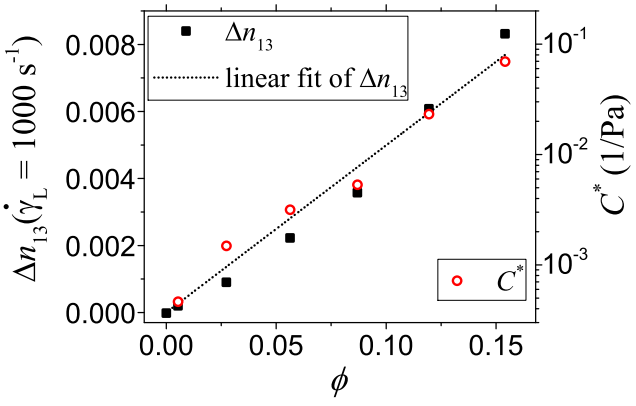

Fig. 9. The effective optical anisotropy Δn_{13} measured at (left axis) and the effective stress-optical coefficient C^* (right axis) as functions of the volume fraction ϕ.

semilogarithmic plot (right vertical axis - log scale, horizontal axis - lin scale), the relationship for $C^*(\phi)$ is approximately linear, meaning that at higher volume fractions, the increase in the effective stress-optical coefficient becomes larger, nearly exponential. We think that this behaviour is related to the emergence of the nematic phase at higher volume fractions.

The effective stress-optical coefficient C^* is already $4.6 \cdot 10^{-4}$ Pa^{-1} at a concentration of ϕ=0.005, and increases with concentration reaching $2.3 \cdot 10^{-2}$ Pa^{-1} at ϕ=0.119, which is still below the isotropic - nematic transition. This is several orders of magnitude higher compared to the earlier findings on other systems. The previously reported systems include the isotropic phase of small molecular bent-core liquid crystalline compounds ($C \approx 7 \cdot 10^{-6}$ Pa^{-1}) [19], liquid crystalline polymers ($C \approx 10^{-6}$ Pa^{-1}) [20,21] or micellar systems ($C \approx 10^{-7}$ Pa^{-1}) [88]. Further, in a PBLG [poly(γ-benzyl L-glutamate)] solution where the nematic transition takes place at ϕ=0.13, C was in the range of 5×10^{-7} Pa^{-1} below ϕ=0.05, and jumped up to 10^{-6} Pa^{-1} at ϕ=0.1 [16] approaching the nematic transition.

The observed large birefringence involves the contribution of several effects. (i) The dispersed pigment particles exhibit intrinsic birefringence because of their crystal structure is orthorhombic with $P2_12_12_1$ symmetry [89]. Moreover the laser wavelength we applied is near the absorption band of the pigment [23], so the resulting resonance in one refractive index may lead to especially high intrinsic birefringence. (ii) The anisotropic polarizability and shape lead to the appearance of scattering birefringence [90,91], which can be described by Mie scattering since the size of the particles is comparable to the wavelength of light. (iii) On the one hand, the quantities of the polymeric dispersant and the pigment particles are almost the same in the suspensions (R_{wd}= 70 wt%, see the experimental section), therefore one may think that the polymeric contribution to the shear-induced birefringence might also be important. We can exclude this effect, however, because the rheo-optical measurements on the 28 wt% solution of Solsperse in dodecane showed undetectable flow-induced birefringence. On the other hand, the polymers adsorbed at the pigment particles may act as a source of interaction between the particles. If the polymer conformation is extended, then the range of the steric interaction among the pigment particles can be relatively large, thus the coupling between shear and orientational order is strong, resulting in an unprecedentedly large effective stress-optical coefficient.

In future studies, it would be interesting to investigate other rheological quantities such as normal stress differences, which could provide further information on the complex particle-particle interactions during shear. Also, other types of colloids with high intrinsic birefringence are potential candidates for strong flow-induced birefringence [92–94]. More data on such systems should shed light on the role of the key parameters (e.g. particle size, shape, crystal properties) in the appearance of a very strong stress-optical response, one example is the suspension of elongated pigment particles presented here.

5. Summary

We investigated rheological, viscoelastic and rheo-optical properties of a dispersion of anisometric pigment particles at various volume fractions. We demonstrated a non-Newtonian flow behaviour transformed into a viscoelastic response with a high storage modulus. This indicates, that the nematic-like state represents a gel state, where the orientational motion of the particles is arrested. One of the main findings is a giant effective stress-optical coefficient, responsible for the flow alignment, which is several orders of magnitude higher than in the other reported cases.

CRediT authorship contribution statement

Péter Salamon: Methodology, Software, Investigation, Writing - original draft. **Yong Geng:** Investigation. **Alexey Eremin:** Conceptualization, Writing - review & editing. **Ralf Stannarius:** Conceptualization, Writing - review & editing. **Susanne Klein:** Resources, Writing - review & editing. **Tamás Börzsönyi:** Conceptualization, Writing - review & editing.

Declaration of competing interest

The authors declare that they have no known competing financial interests or personal relationships that could have appeared to influence the work reported in this paper.

Acknowledgement

Financial support from the DAAD/Tempus researcher exchange program (Grant No. 274464), the COST Action IC1208, the grants NKFIH K116036, PD121019, FK125134, and DFG (STA 425/36 within SPP 1681) are acknowledged.

References

[1] R.G. Larson, The Structure and Rheology of Complex Fluids, Oxford University Press, 1998.
[2] J. Mewis, N.J. Wagner, Colloidal Suspension Rheology, Cambridge University Press, Cambridge, United Kingdom, 2012.
[3] A.R. Altenberger, J.S. Dahler, On the kinetic theory and rheology of a solution of rigid-rodlike macromolecules, Macromolecules 18 (9) (1985) 1700–1710.
[4] J. Araki, M. Wada, S. Kuga, T. Okano, Influence of surface charge on viscosity behavior of cellulose microcrystal suspension, J. Wood Sci. 45 (3) (1999) 258–261.
[5] V.N. Tsvetkov, Flow birefringence and the structure of macromolecules, Sov. Phys. Uspekhi 6 (5) (1964) 639–681.
[6] J.L.S. Wales, The Application of Flow Birefringence to Rheological Studies of Polymer Melts, Delft University Press, 1976.
[7] H. Janeschitz-Kriegl, Polymer Melt Rheology and Flow Birefringence, Vol. 6 of Polymers/Properties and Applications, Springer-Verlag Berlin Heidelberg, 1983.
[8] J.W. Bender, N.J. Wagner, Optical measurement of the contributions of colloidal forces to the rheology of concentrated suspensions, J. Colloid Interface Sci. 172 (1) (1995) 171–184.
[9] J. Vermant, H. Yang, G. Fuller, Rheooptical determination of aspect ratio and polydispersity of nonspherical particles, AICHE J. 47 (4) (2001) 790–798.
[10] P. Kahl, L. Noirez, From flow birefringence in the isotropic phase of liquid crystals to the identification of shear elasticity in liquids, Liquid Crystal Reviews 4 (2) (2016) 137.
[11] R.H. Marchessault, F.F. Morehead, M.J. Koch, Some hydrodynamic properties of neutral suspensions of cellulose crystallites as related to size and shape, J. Colloid Sci. 16 (4) (1961) 327–344.
[12] R.H. Marchessault, M.J. Koch, J.T. Yang, Some hydrodynamic properties of ramie crystallites in phosphate buffer, J. Colloid Sci. 16 (4) (1961) 345–360.
[13] E.K. Hobbie, Optical anisotropy of nanotube suspensions, J. Chem. Phys. 121 (2) (2004) 1029–1037.
[14] S. Chu, S. Venkatraman, G.C. Berry, Y. Einaga, Rheological properties of rodlike polymers in solution. 1. Linear and nonlinear steady-state behavior, Macromolecules 14 (4) (1981) 939–946.
[15] S. Venkatraman, G.C. Berry, Y. Einaga, Rheological properties of rodlike polymers in solutions - 2. Linear and nonlinear transient behaviour, J. Polymer Science. Part A-2, Polymer Physics 23 (7) (1985) 1275–1295.
[16] D.W. Mead, R.G. Larson, Rheooptical study of isotropic solutions of stiff polymers, Macromolecules 23 (9) (1990) 2524–2533.
[17] H. Thurn, M. Löbl, H. Hoffmann, Viscoelastic detergent solutions. A quantitative comparison between theory and experiment, J. Phys. Chem. 89 (3) (1985) 517–522.
[18] B.A. Schubert, E.W. Kaler, N.J. Wagner, The microstructure and rheology of mixed cationic/anionic wormlike micelles, Langmuir 19 (10) (2003) 4079–4089.
[19] C. Bailey, K. Fodor-Csorba, R. Verduzco, J.T. Gleeson, S. Sprunt, A. Jákli, Large flow birefringence of nematogenic bent-core liquid crystals, Phys. Rev. Lett. 103 (23) (2009), 237803. .
[20] C. Pujolle-Robic, L. Noirez, Observation of shear-induced nematic-isotropic transition in side-chain liquid crystal polymers, Nature 409 (6817) (2001) 167–171.
[21] C. Pujolle-Robic, L. Noirez, Identification of nonmonotonic behaviors and stick-slip transition in liquid crystal polymers, Phys. Rev. E 68 (2003), 061706. .
[22] J. Heuer, I. Niskanen, S. Klein, Peiponen, optical properties of suspensions of organic and inorganic red pigments, Appl. Spectroscopy 65 (2011) 1181–1186.
[23] A. Eremin, R. Stannarius, S. Klein, J. Heuer, R.M. Richardson, Switching of electrically responsive, light-sensitive colloidal suspensions of anisotropic pigment particles, Adv. Funct. Mat. 21 (3) (2011) 556–564.
[24] R.J. Greasty, R.M. Richardson, S. Klein, D. Cherns, M.R. Thomas, C. Pizzey, N. Terrill, C. Rochas, Electro-induced orientational ordering of anisotropic pigment nanoparticles, Phil. Trans. Roy. Soc. London A: Mathematical, Physical and Engineering Sciences 371 (1988) (2013) 20120257.

[25] K. May, R. Stannarius, S. Klein, A. Eremin, Electric-field-induced phase separation and homogenization dynamics in colloidal suspensions of dichroic rod-shaped pigment particles, Langmuir 30 (24) (2014) 7070–7076.
[26] S. Kredentser, A. Eremin, P. Davidson, V. Reshetnyak, R. Stannarius, Y. Reznikov, Light-induced soret effect and adsorption of nanocrystals in organic solvents, Eur. Phys. J. E 39 (2016) 38.
[27] K. May, A. Eremin, R. Stannarius, S. Peroukidis, S. Klapp, S. Klein, Colloidal suspensions of rodlike nanocrystals and magnetic spheres under an external magnetic stimulus: experiment and molecular dynamics simulation, Langmuir 32 (20) (2016) 5085–5093.
[28] C. Gähwiller, Temperature dependence of flow alignment in nematic liquid crystals, Phys. Rev. Lett. 28 (1972) 1554.
[29] F.M. Leslie, Theory of flow phenomena in liquid crystals, Adv. Liq. Cryst. 4 (1979) 1.
[30] T. Börzsönyi, B. Szabó, G. Törös, S. Wegner, J. Török, E. Somfai, T. Bien, R. Stannarius, Orientational order and alignment of elongated particles induced by shear, Phys. Rev. Lett. 108 (2012), 228302. .
[31] E.J. Hinch, L.G. Leal, The effect of brownian motion on the rheological properties of a suspension of non-spherical particles, J. Fluid Mech. 52 (4) (1972) 683–712.
[32] L. Onsager, The effects of shape on the interaction of colloidal particles, Ann. N. Y. Acad. Sci. 51 (1949) 627–659.
[33] G.J. Vroege, H.N.W. Lekkerkerker, Phase transitions in lyotropic colloidal and polymer liquid crystals, Rep. Prog. Phys. 55 (8) (1992) 1241–1309.
[34] A. Speranza, P. Sollich, Isotropic-nematic phase equilibria in the onsager theory of hard rods with length polydispersity, Phys. Rev. E 67 (6 1) (2003) 061702/1–061702/19.
[35] J. Tang, S. Fraden, Isotropic-cholesteric phase transition in colloidal suspensions of filamentous bacteriophage fd, Liq. Cryst. 19 (4) (1995) 459–467.
[36] J. Li, J. Revol, R.H. Marchessault, Rheological properties of aqueous suspensions of chitin crystallites, J. Colloid Interf. Sci. 183 (2) (1996) 365–373.
[37] L. Li, J. Walda, L. Manna, A.P. Alivisatos, Semiconductor nanorod liquid crystals, Nano Lett. 2 (6) (2002) 557–560.
[38] H. Maeda, Y. Maeda, Liquid crystal formation in suspensions of hard rodlike colloidal particles: direct observation of particle arrangement and self-ordering behavior, Phys. Rev. Lett. 90 (2003), 018303. .
[39] L. Li, M. Marjanska, G.H.J. Park, A. Pines, A.P. Alivisatos, Isotropic-liquid crystalline phase diagram of a cdse nanorod solution, J. Chem. Phys. 120 (3) (2004) 1149–1152.
[40] V.A. Davis, L.M. Ericson, A.N.G. Parra-Vasquez, H. Fan, Y. Wang, V. Prieto, J.A. Longoria, S. Ramesh, R.K. Saini, C. Kittrell, W.E. Billups, W.W. Adams, R.H. Hauge, R.E. Smalley, M. Pasquali, Phase behavior and rheology of swnts in superacids, Macromolecules 37 (1) (2004) 154–160.
[41] M.P. Lettinga, J.K.G. Dhont, Non-equilibrium phase behaviour of rod-like viruses under shear flow, J. Phys. Cond. Matter 16 (38) (2004) S3929–S3939.
[42] M.P. Lettinga, Z. Dogic, H. Wang, J. Vermant, Flow behavior of colloidal rodlike viruses in the nematic phase, Langmuir 21 (17) (2005) 8048–8057.
[43] P. Davidson, J..P. Gabriel, Mineral liquid crystals, Curr. Opinion Colloid and Interf. Sci. 9 (6) (2005) 377–383.
[44] L. Michot, I. Bihannic, S. Maddi, S. Funari, C. Baravian, P. Levitz, P. Davidson, Liquid-crystalline aqueous clay suspension, Proc. Natl. Acad. Sci. U. S. A. 103 (44) (2006) 16101–16104.
[45] G. Vroege, D. Thies-Weesie, A. Petukhov, B. Lemaire, P. Davidson, Smectic liquid-crystalline order in suspensions of highly polydisperse goethite nanorods, Adv. Mater. 18 (19) (2006) 2565–2568.
[46] B. Ruzicka, E. Zaccarelli, A fresh look at the laponite phase diagram, Soft Matter 7 (4) (2011) 1268–1286.
[47] E.E. Urena-Benavides, G. Ao, V.A. Davis, C.L. Kitchens, Rheology and phase behavior of lyotropic cellulose nanocrystal suspensions, Macromolecules 44 (22) (2011) 8990–8998.
[48] L. Bailey, H. Lekkerkerker, G. Maitland, Smectite clay-inorganic nanoparticle mixed suspensions: phase behaviour and rheology, Soft Matter 11 (2) (2015) 222–236.
[49] P.D. Olmsted, P. Goldbart, Theory of the nonequilibrium phase transition for nematic liquid crystals under shear flow, Phys. Rev. A 41 (8) (1990) 4578–4581.
[50] P.D. Olmsted, P.M. Goldbart, Isotropic-nematic transition in shear flow: state selection, coexistence, phase transitions, and critical behavior, Phys. Rev. A 46 (8) (1992) 4966–4993.
[51] X. Yuan, M.P. Allen, Non-linear responses of the hard-spheroid fluid under shear flow, Physica A 240 (1–2) (1997) 145–159.
[52] R.J. Greasty, Orientational Order in Pigment Particle Suspensions, Ph.D. thesis University of Bristol, 2012.
[53] I.R. Rutgers, Relative viscosity of suspensions of rigid spheres in Newtonian liquids, Rheol. Acta 2 (3) (1962) 202–210.
[54] D.G. Thomas, Transport characteristics of suspension: Viii. A note on the viscosity of newtonian suspensions of uniform spherical particles, J. Colloid Sci. 20 (3) (1965) 267–277.
[55] D.J. Jeffrey, A. Acrivos, The rheological properties of suspensions of rigid particles, AIChE Journal 22 (3) (1976) 417–432.
[56] A.B. Metzner, Rheology of suspensions in polymeric liquids, J. Rheol. 29 (6) (1985) 739–775.
[57] C.W. Macosko, Rheology: Principles, Measurements, and Applications, Wiley-VCH, 1994.
[58] A.M. Wierenga, A.P. Philipse, Low-shear viscosity of isotropic dispersions of (brownian) rods and fibres; a review of theory and experiments, Colloids and Surfaces A 137 (1–3) (1998) 355–372.
[59] M.M. Cross, Rheology of synthetic latices: influence of shear rate and temperature, J. Colloid Interf. Sci. 44 (1) (1973) 175–176.
[60] S. Hess, Viscoelasticity associated with molecular alignment, Z. Naturforsch. A 35 (9) (1980) 915–919.
[61] L.M. Walker, N.J. Wagner, R.G. Larson, P.A. Mirau, P. Moldenaers, The rheology of highly concentrated pblg solutions, J. Rheol. 39 (5) (1995) 925–952.
[62] L.M. Walker, W.A. Kernick III, N.J. Wagner, In situ analysis of the defect texture in liquid crystal polymer solutions under shear, Macromolecules 30 (3) (1997) 508–514.
[63] H. Lee, D.A. Brant, Rheology of concentrated isotropic and anisotropic xanthan solutions. 1. A rodlike low molecular weight sample, Macromolecules 35 (6) (2002) 2212–2222.
[64] H. Lee, D.A. Brant, Rheology of concentrated isotropic and anisotropic xanthan solutions. 2. A semiflexible wormlike intermediate molecular weight sample, Macromolecules 35 (6) (2002) 2223–2234.
[65] M.M. De Souza Lima, R. Borsali, Rodlike cellulose microcrystals: structure, properties, and applications, Macromol. Rapid Comm. 25 (7) (2004) 771–787.
[66] S. Shafiei-Sabet, W.Y. Hamad, S.G. Hatzikiriakos, Rheology of nanocrystalline cellulose aqueous suspensions, Langmuir 28 (49) (2012) 17124–17133.
[67] A. Lu, U. Hemraz, Z. Khalili, Y. Boluk, Unique viscoelastic behaviors of colloidal nanocrystalline cellulose aqueous suspensions, Cellulose 21 (3) (2014) 1239–1250.
[68] N. Quennouz, S.M. Hashmi, H.S. Choi, J.W. Kim, C.O. Osuji, Rheology of cellulose nanofibrils in the presence of surfactants, Soft Matter 12 (1) (2015) 157–164.
[69] T.G. Mezger, The Rheology Handbook, 4th edition Vincentz Network GmbH & Co. KG, Hanover, 2014.
[70] I.M. Krieger, T.J. Dougherty, A mechanism for non-Newtonian flow in suspensions of rigid spheres, J. Rheol. 3 (1) (1959) 137–152.
[71] G.D.J. Phillies, P. Peczak, The ubiquity of stretched-exponential forms in polymer dynamics, Macromolecules 21 (1) (1988) 214–220.
[72] C. Graf, H. Kramer, M. Deggelmann, M. Hagenbüchle, C. Johner, C. Martin, R. Weber, Rheological properties of suspensions of interacting rodlike fd-virus particles, J. Chem. Phys. 98 (6) (1993) 4920–4928.
[73] W. Pabst, E. Gregorova, C. Berthold, Particle shape and suspension rheology of short-fiber systems, J. Eur. Ceramic Soc. 26 (1–2) (2006) 149–160.
[74] M.J. Solomon, D.V. Boger, The rheology of aqueous dispersions of spindle-type colloidal hematite rods, J. Rheol. 42 (4) (1998) 929–949.
[75] W. Kuhn, H. Kuhn, Die Abhängigkeit der Viskosität vom Strömungsgefälle bei hochverdünnten Suspensionen und Lösungen, Helv. Chim. Acta. 28 (1945) 97–127.
[76] H. Brenner, Rheology of a dilute suspension of axisymmetric Brownian particles, Int. J. Multiphase Flow 1 (2) (1974) 195–341.
[77] H.A. Scheraga, Non-Newtonian viscosity of solutions of ellipsoidal particles, J. Chem. Phys. 23 (8) (1955) 1526–1532.
[78] J. Royer, G. Burton, D. Blair, S. Hudson, Rheology and dynamics of colloidal superballs, Soft Matter 11 (28) (2015) 5656–5665.
[79] C. Cwalina, K. Harrison, N. Wagner, Rheology of cubic particles suspended in a Newtonian fluid, Soft Matter 12 (20) (2016) 4654–4665.
[80] J. Araki, M. Wada, S. Kuga, T. Okano, Flow properties of microcrystalline cellulose suspension prepared by acid treatment of native cellulose, Colloids Surf. A Physicochem. Eng. Asp. 142 (1) (1998) 75–82.
[81] R. Simha, The influence of Brownian movement on the viscosity of solutions, J. Phys. Chem. 44 (1) (1940) 25–34.
[82] S. Haber, H. Brenner, Rheological properties of dilute suspensions of centrally symmetric Brownian particles at small shear rates, J. Coll. Interf. Sci. 97 (2) (1984) 496–514.
[83] M. Bercea, P. Navard, Shear dynamics of aqueous suspensions of cellulose whiskers, Macromolecules 33 (16) (2000) 6011–6016.
[84] F. Martoia, C. Perge, P. Dumont, L. Orgeas, M. Fardin, S. Manneville, M. Belgacem, Heterogeneous flow kinematics of cellulose nanofibril suspensions under shear, Soft Matter 11 (24) (2015) 4742–4755.
[85] F. Martoia, P. Dumont, L. Orgeas, M. Belgacem, J.-L. Putaux, Micro-mechanics of electrostatically stabilized suspensions of cellulose nanofibrils under steady state shear flow, Soft Matter 12 (6) (2016) 1721–1735.
[86] K. Miyazaki, H.M. Wyss, D.A. Weitz, D.R. Reichman, Nonlinear viscoelasticity of metastable complex fluids, Europhys. Lett. 75 (6) (2006) 915–921.
[87] S. Srivastava, J.H. Shin, L.A. Archer, Structure and rheology of nanoparticle-polymer suspensions, Soft Matter 8 (2012) 4097.
[88] B.D. Frounfelker, G.C. Kalur, B.H. Cipriano, D. Danino, S.R. Raghavan, Persistence of birefringence in sheared solutions of wormlike micelles, Langmuir 25 (1) (2009) 167–172.
[89] M. Schmidt, D. Hofmann, C. Buchsbaum, H. Metz, Crystal structures of pigment red 170 and derivatives, as determined by x-ray powder diffraction, Angewandte Chemie - International Edition 45 (8) (2006) 1313–1317.
[90] S.J. Johnson, G.G. Fuller, The optical anisotropy of sheared hematite suspensions, J. Colloid Interf. Sci. 124 (2) (1988) 441–451.
[91] G.G. Fuller, Optical Rheometry of Complex Fluids, Oxford University Press, 1995.
[92] K. Sandomirski, S. Martin, G. Maret, H. Stark, T. Gisler, Highly birefringent colloidal particles for tracer studies, Journal of Physics Condensed Matter 16 (38) (2004) S4137–S4144.
[93] R. Piazza, V. Degiorgio, Dynamic light scattering study of colloidal crystals made of anisotropic spherical latex particles, Physica A: Statistical Mechanics and its Applications 182 (4) (1992) 576–592.
[94] V. Degiorgio, R. Piazza, T. Bellini, Static and dynamic light scattering study of fluorinated polymer colloids with a crystalline internal structure, Adv. Colloid Interf. Sci. 48 (C) (1994) 61–91.